RSC Advances

ROYAL SOCIETY OF CHEMISTRY

www.rsc.org/advances

Journal Name

ARTICLE

Enhanced electrochemical performance of vanadium dioxide (B) nanoflowers by graphene nanoribbons support

Received 00th January 20xx,
Accepted 00th January 20xx

DOI: 10.1039/x0xx00000x

www.rsc.org/

Zihan Fan, Lina Jia, Cunli Lin, Xiangyue Huang, Xiaolin Hu,* Naifeng Zhuang, and Jianzhong Chen

Specific VO_2(B) nanoflower and its composite hybridized with graphene nanoribbons (GNRs) are prepared by using moderate $H_2C_2O_4$ reductant to reduce V_2O_5 with the mole ratio of $H_2C_2O_4$:V_2O_5 at 3:1. The discharge specific capacities and the cycling stabilities of VO_2(B) cathode material for lithium-ion battery can be improved by graphene support. Especially GNRs support can improve the dispersibility and the electrical conductivity of VO_2(B) nanoflower. Thus, VO_2(B)/GNRs (32.2 wt%) exhibits excellent electrochemical performance with high specific capacity of 471.5 mAh g^{-1} and preferable cycling stability.

Introduction

Lithium-ion batteries (LIBs) have been a favorable portable power source device in electronics and electric vehicles because of the high capacity, long cycle life, environmental benignity, low self-discharge and so on.[1] The commercial LIBs presently use $LiCoO_2$ as the cathode, but only 50% of its theoretical capacity could be practically utilized (140 mAh g^{-1}) [2,3]. It is unable to meet the requirements of the further miniaturization of electronic equipment and the high energy density and high rate capability of large power equipment.[2] In addition, the specific capacity of existing cathode material is difficult to be increased because of the limitation of theoretical capacity. Therefore, it is important to find other cathode substitutes instead of $LiCoO_2$ for LIBs.

Recently, the transition-metal oxides have attracted extensive attention and are expected to be used as cathode materials in the next generation rechargeable batteries, for example, MnO_2,[4] VO_x,[5-9] MoO_3,[9,10] or Fe_2O_3.[11] Among these candidates, vanadium oxide has been considered to be the most promising candidate, owing to its layer structure, in which the atoms link each other by covalently bonds to form two dimensional layers that are stacked together through the weak Van der Waals interaction.[9,12-14] The weak interaction allows the foreign ion or molecule to be introduced into the interlayer. Moreover, vanadium oxide has good reactive activity due to the various oxidation states of vanadium from +2 in VO to +5 in V_2O_5.[14-17] V_2O_5 has a series of phase transformation during Li^+ intercalation/deintercalation process. For the different intercalated amounts of Li^+, the theoretical capacities could be up to 294 mAh g^{-1} for $Li_2V_2O_5$ and 442 mAh g^{-1} for $Li_3V_2O_5$, respectively.[14,18] However, $Li_xV_2O_5$ with a intercalated amount x > 1 suffers a great loss of capacity during the charge and discharge process, which affects the battery cycling performance. Compared to V_2O_5, VO_2(B) nanomaterial with a metastable monoclinic structure is found to be a excellent promising electrode material owing to not only its high theoretical capacity of 320 mAh g^{-1},[19] but also its tunnel structure, through which lithium ions can easily intercalate and deintercalate in LIBs.[19-21] Current research results show the specific discharge capacity of VO_2(B) is 152-450 mAh g^{-1} at the low current density of 10 mA g^{-1} and less than 200 mAh g^{-1} at the high current density of 100 mA g^{-1},[22-29] which are all higher than that of $LiCoO_2$ cathode. But the large irreversible capacity loss, poor cycling stability and low rate capability are the critical drawbacks those can lead to the poor capacity retention. These drawbacks mainly result from the intrinsic poor conductivity and the aggregation of nanometer electrode material during the electrochemical cycling process.[30]

To improve the conductivity and dispersibility of cathode material and effectively enhance the electrochemical performance, many researchers are devoted to construct composite structures of electrode material with polypyrrole,[31,32] carbon nanotube,[33-37] graphene,[38,39] and so on. Compared with VO_2 material, the composites of VO_2(B) with carbon nanotube and graphene exhibit the superior performance and the capacity retention ratios.[37-39] Graphene nanoribbon (GNR) has a quasi-one-dimension structure with large specific surface areas and high electrical conductivity.[40-42] The large length-diameter ratio makes GNRs easily twist to network structure with a lot of void space, which is conducive to rapid diffusion of electrolyte, accelerate the adsorption and desorption of Li ion and then improve the charge-discharge efficiency of LIBs.[43] Therefore, in this paper, GNRs were used to support VO_2(B) nanoflower to improve the charge-discharge cycling stability and increase the specific capacity of Li-VO_2(B) battery.

College of Chemistry, Fuzhou University, Fuzhou 350116, People's Republic of China. E-mail: linamethyst@fzu.edu.cn; Tel/Fax: +86-591-22866130

† Electronic Supplementary Information (ESI) available: Synthesis details and theoretical calculation details. See DOI: 10.1039/x0xx00000x

Experimental

Preparation of VO_2(B)

VO_2(B) crystallites were synthesized by the hydrothermal method. 20 mg vanadium pentoxide (V_2O_5) were dissolved into 16 ml deionization (DI) water with a certain quality of oxalic acid ($H_2C_2O_4$, the mole ratio of $H_2C_2O_4$:V_2O_5 is 1:1, 2:1 and 3:1 respectively) or 50 μl 0.01% hydrazine hydrate solution. The mixed solution was put into a 20 ml Teflon-lined autoclave and heated at 180 °C for 5-48 h. Then, the autoclave was cooled to room temperature. The dark blue precipitate was collected by centrifugation, washed thoroughly with DI water and anhydrous ethanol, and finally dried at 60 °C for 12 h in a vacuum.

Preparation of VO_2(B)/GNRs

20 mg V_2O_5 and 41 mg $H_2C_2O_4$ were dissolved into 16 ml DI water to obtain light green solution. Then, GNRs was added into the solution. After being stirred uniformly, the liquid mixture was put into a 20 ml Teflon-lined autoclave and heated at 180 °C for 5 h or 24 h. The blue-black precipitate was collected by centrifugation, washed thoroughly with DI water and anhydrous ethanol, and then dried at 60 °C for 12 h in a vacuum. Finally, the composite of GNRs supported VO_2(B) nanomaterials (denoted as VO_2(B)/GNRs) was obtained. Here the weight percentage of GNRs in the composite is 32.2 wt%. In order to evaluate the electrochemical performance of VO_2(B)/GNRs, the graphene sheets (GSs) was also used as the carrier to prepare VO_2(B)/GSs (32.2 wt%) composite by the similar method.

In order to investigate the impact of GNRs component on the electrochemical performance, the composites with the different weight percentages of GNRs were prepared. These composites are marked as VO_2(B)/GNRs (7.4 wt%), VO_2(B)/GNRs (24.8 wt%), VO_2(B)/GNRs (32.2 wt%) and VO_2(B)/GNRs (35.7 wt%) according to the weight percentages of GNRs.

Physical and electrochemical characterization

Crystallographic informations for the samples were analyzed by using the powder X-ray diffraction (XRD) meter (Rigaku D/max-3C) with Cu K_α radiation (λ = 1.5418 Å), the graphite monochromator, and the working voltage of 35 kV. The morphologies were investigated by using scanning electron microscopy (SEM, HIROX SH-4000) and transmission electron microscopy (TEM, American FEI, G2 F20 S-TWIN) with an acceleration voltage of 200 kV.

The electrochemical measurements were carried out by using LAND Systems (Shanghai Chenhua CHI660C). The surface of aluminum sheet with the diameter of 1 cm was ultrasonic cleaned with acetone for 30 min. Then the aluminum sheet was washed with DI water by using ultrasonic assistance. The working electrode consisted of the active composite material (VO_2(B)/GNRs), a conductive agent (Super-P), and a polymer binder (polyvinylidene fluoride, PVDF) in a weight ratio of 8:1:1. These materials were grinded and mixed uniformly, and formed the homogeneous slurry with adding N-methyl pyrrolidone. The slurry was then covered onto the aluminum sheet. The coated electrode was dried at 80 °C for 10 h in vacuum. The button battery was assembled in a glove box filled with argon atmosphere. The counter electrode was Li metal. The electrolyte was $LiPF_6$ (1.0 M) in a 50:50 (w/w) mixture of ethylene carbonate (EC) and diethyl carbonate (DEC). The diaphragm was Cellgard 2400. The button battery was charged and discharged galvanostatically at the current density of 40 mA g^{-1} in the voltage range of 0.01–4 V to measure the electrochemical response at room temperature. The rate performance was tested at various current rates.

Results and discussions

Phase analysis and morphology of VO_2(B)

The crystal phase analysis of as-prepared VO_2(B) shown in Fig. S1 and Fig. S2 (see ESI) indicates that the reducibility of hydrazine hydrate is so strong that V_2O_5 is restored to the varied vanadium oxides. It is appropriate to choose oxalic acid as the reductant, which reduces V_2O_5 to a single VO_2(B) phase without impurity phases.

On the other hand, the dosage of oxalic acid has a significant impact on the crystal phase and the morphology of vanadium oxide. Fig. 1 shows that the as-prepared vanadium oxide has the impurity diffraction peaks at 2θ angles of 13.0°, 26.7°, 31.0° and 45.6° assigned to the vanadium oxides including V_4O_9 (JCPDS 71-2248), V_6O_{13} (JCPDS 89-0100) and V_2O_5 (JCPDS 77-2418) except the diffraction patterns of VO_2(B) (JCPDS 81-2392) when the mole ratio of $H_2C_2O_4$:V_2O_5 is 1:1. It is mainly because that the low concentration of $H_2C_2O_4$ reductant can not completely restore V_2O_5. As shown in the SEM images (see Fig. 2a), the as-prepared acicular- or stick-like VO_2 agglomerate with the unreacted V_2O_5 and other miscellaneous vanadium oxides. When the mole ratio of $H_2C_2O_4$:V_2O_5 reaches at 2:1 and 3:1, XRD patterns of products match well with the monoclinic phase of VO_2(B) (JCPDS 81-2392). Increasing the reductant concentration can improve the crystallinity of VO_2(B) and obviously enhance the strength of diffraction peak at a 2θ of 25.2°. It indicates that VO_2(B) grows preferentially along (110) direction. SEM image (Fig. 2b) shows that the as-prepared VO_2(B) is still acicular- or stick-like shape but has apparently dispersed when $H_2C_2O_4$:V_2O_5 is 2:1. Moreover when $H_2C_2O_4$:V_2O_5 is 3:1, VO_2(B) shows the flower- or carambola-like shape (see Fig. 2c and d) with the large specific surface area and the better dispersion. It indicates that VO_2(B) would have good electrochemical performance. Therefore, we would further prepare VO_2(B) nanoflowers and focus on the effect of GNRs support on their electrochemical performance.

Phase analysis and morphology of VO_2(B)/GNRs

In order to improve the electrochemical performance of VO_2(B), the composite of VO_2(B) nanoflower supported with GNRs (VO_2(B)/GNRs) has been prepared. XRD patterns and TEM images are shown in Fig. 3 and Fig. 4. There is a broad characteristic diffraction peak of GNRs at 2θ = 26°. When the

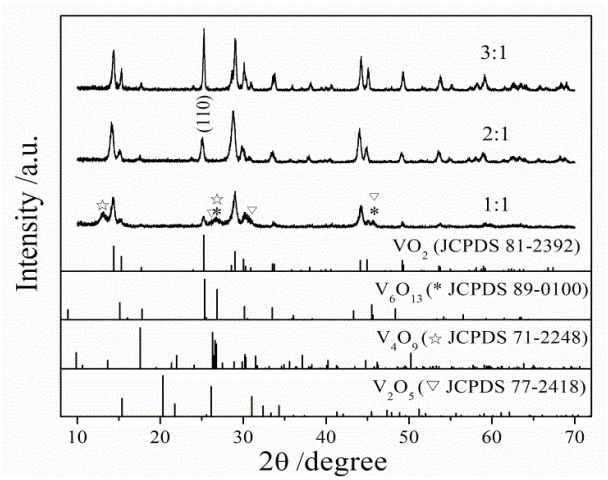

Fig. 1 XRD patterns of as-prepared vanadium oxides with different mole ratios of $H_2C_2O_4$:V_2O_5.

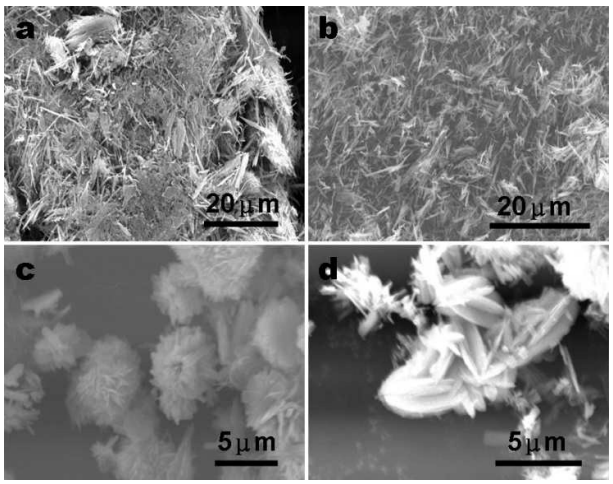

Fig. 2 SEM images of as-prepared vanadium oxides with the different mole ratios of $H_2C_2O_4$:V_2O_5. $H_2C_2O_4$:V_2O_5 is 1:1 (a), 2:1 (b), 3:1 (c & d).

reaction time is 5 h, the as-prepared product is a mixture of vanadium oxides. Fig. 4a and b show that the mixture of vanadium oxide with the average particle size of 5-10 nm supports with GNRs (V_xO_y/GNRs). When the reaction time reaches to 24 h, the single-phase VO_2(B) with the strip-like morphology can be obtained as shown in Fig. 4c-e. VO_2(B) strip and GNRs interact with each other to gather into a blossoming flower. The flower structure with a certain interspace and a big specific surface area is beneficial to the rapid diffusion of electrolyst and the intercalation/deintercalation of Li^+ ion. GNR support may improve the dispersibility of VO_2(B) strip and avoid the agglomeration. Compared with VO_2(B)/GNRs, most of VO_2(B) strips or rods scatter around GSs without close interaction, as shown in SEM image of Fig. 4f.

Electrochemical characterization

Graphene has a variety of structures including nanosheet and

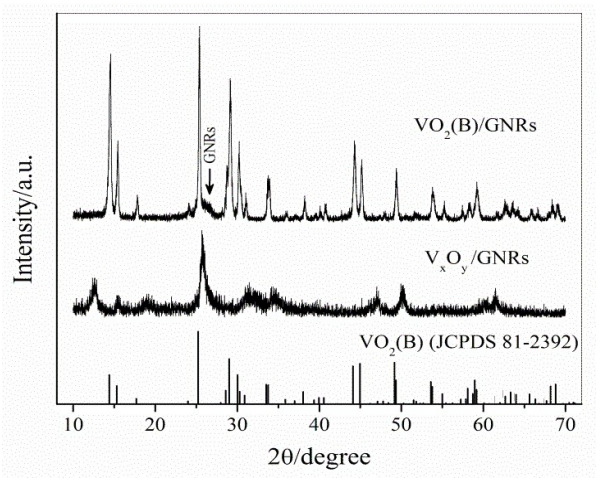

Fig. 3 XRD patterns of vanadium oxide/GNRs composites.

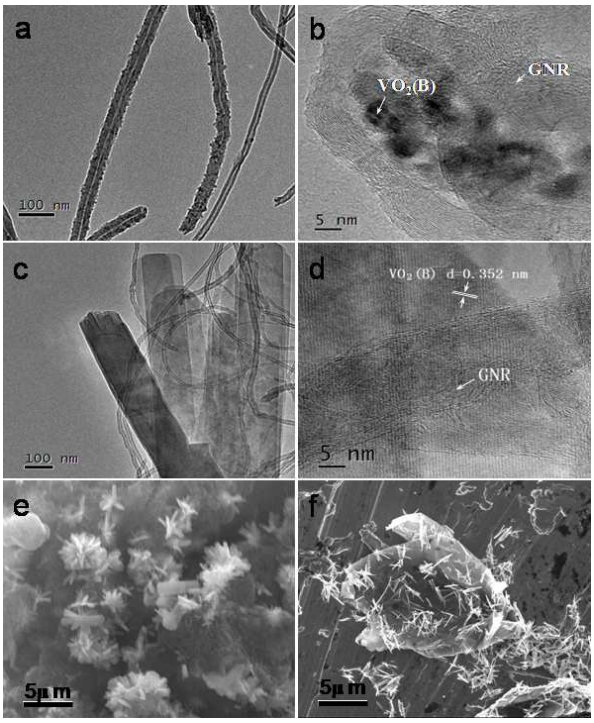

Fig. 4 TEM (a) and HRTEM (b) images of V_xO_y/GNRs; TEM (c), HRTEM (d) and SEM (e) images of VO_2(B)/GNRs; SEM image (f) of VO_2(B)/GSs.

nanoribbon, whose electrical conductivities are different and their impacts on the electrochemical performance of VO_2(B) are not entirely consistent. The excellent electrical property of GNR help enhance the electrical conductivity of VO_2(B) and increase specific capacity. Different from the chaotic mobility towards different direction on the two-dimensional structure of GS, the electron mobility can be accelerated along the longitudinal direction of the quasi-one-dimensional GNR during the charge and discharge process, which will improve the ability of VO_2(B) to store lithium ions and improve the electrochemical reaction rate. As shown in Fig. 5 and Fig. 6,

VO_2(B)/GNRs can obtain better electrochemical performance than VO_2(B)/GSs. Fig. 5 shows that the discharge specific capacity of VO_2(B) is 206.8 mAh g^{-1} at the first cycle and drops to 51.4 mAh g^{-1} at the 2nd cycle, then gradually decreases during the subsequent charge and discharge process. The discharge specific capacity of VO_2(B)/GSs (32.2%) composite is 360.6 mAh g^{-1} at the first cycle and then decreases to 126.8 mAh g^{-1} with the capacity retention rate of 35% after 30 cycles. The charge-discharge coulomb efficiency (Fig. 6d) in the first three cycles is not stable but keeps about 100% in the later cycles. It shows that GSs support can improve the discharge capacity and cycling stability of VO_2(B). But the interaction between VO_2(B) strips or rods and GSs is not close (Fig. 4f). Thus the contribution of GSs does not fully play out for further improving the discharge capacity. Under the same measurement condition, VO_2(B)/GNRs (32.2%) composite exhibits a discharge specific capacity of 471.5 mAh g^{-1} at the first cycle which is higher than VO_2(B) and VO_2(B)/GSs. After 30 cycles, the discharge specific capacity decays to 172.4 mAh g^{-1} with the capacity retention rate of 37%. The coulomb efficiency is about 100% (Fig. 6f). For the case of VO_2(B)/GNRs, the charge-discharge potential-time curve (see Fig. S3) has a symmetry characteristic and a stable charge-discharge time. Therefore, it can be seen that VO_2(B)/GNRs has not only a higher discharge capacity but also a better capacity stability.

Next we focus on the impact of GNRs component on the discharge specific capacity and the cycling stability of VO_2(B)/GNRs composite. The discharge performances of VO_2(B), GNRs, VO_2(B)/GNRs (7.4 wt%), VO_2(B)/GNRs (28.4 wt%), VO_2(B)/GNRs (32.2 wt%), and VO_2(B)/GNRs (35.7 wt%) are shown in Fig. 7. The discharge specific capacity of VO_2(B) nanoflower is 206.8 mAh g^{-1} at the first cycle, then declines fast to 6.5 mAh g^{-1} after 30 cycles with capacity retention rate of only 3%. However, the discharge specific capacities of VO_2(B)/GNRs composites are higher than that of VO_2(B). The first discharge specific capacities of VO_2(B)/GNRs(7.4 wt%), VO_2(B)/GNRs (28.4 wt%), VO_2(B)/GNRs (32.2 wt%), VO_2(B)/GNRs (35.7 wt%) attain 200.2, 303.1, 471.5, 441.7 mAh g^{-1} and decay to 19.5, 94.3, 172.4, 128.2 mAh g^{-1} with a capacity retention rate of 10%, 31%, 37%, 29% after 30 cycles, respectively. It can be found that with the increase of weight percentage of GNRs, the advantage of composite is becoming obvious that the discharge specific capacity and the capacity stability have been improved. But if the weight percentage of GNRs continues to increase, the electrochemical performance of active substance VO_2(B) will be affected.

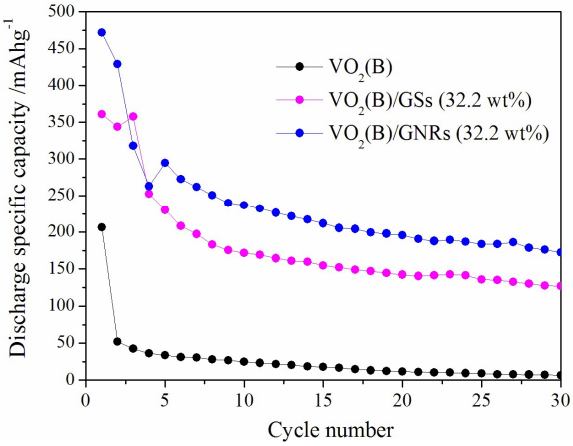

Fig. 5 Discharge specific capacity and cycling performance of as-prepared VO_2(B), VO_2(B)/GSs and VO_2(B)/GNRs.

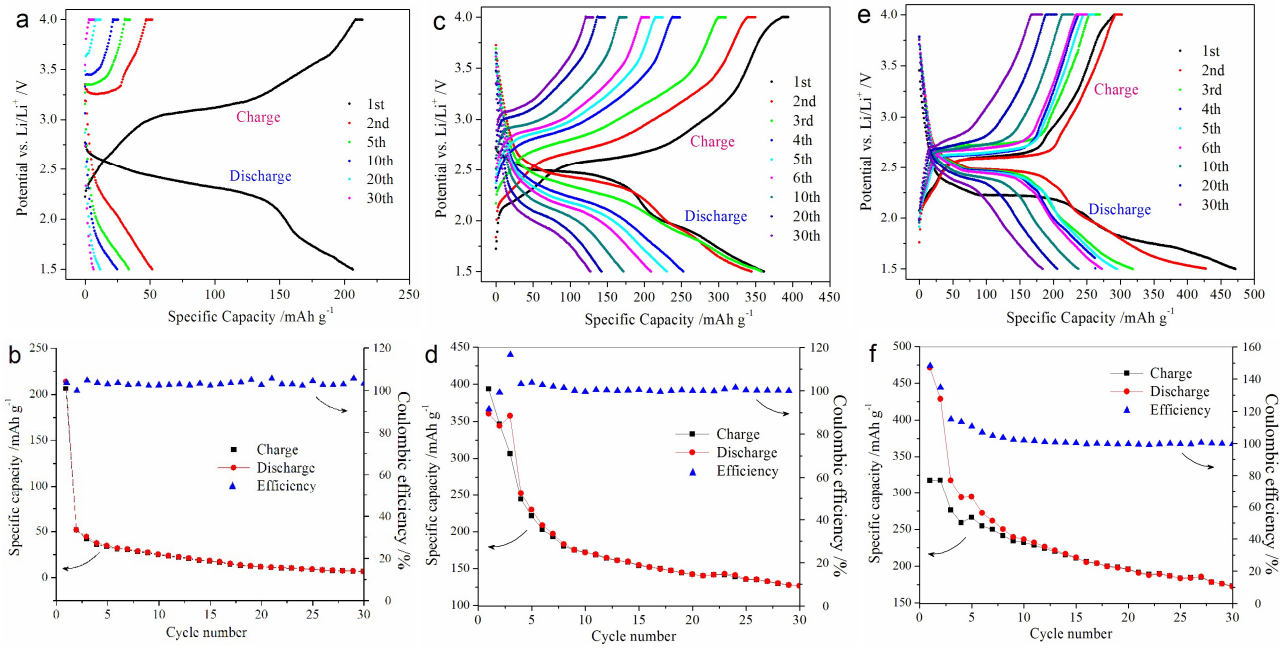

Fig. 6 Charge-discharge curves and coulomb efficiency of as-prepared VO_2(B) (a, b), VO_2(B)/GSs (c, d) and VO_2(B)/GNRs (e, f).

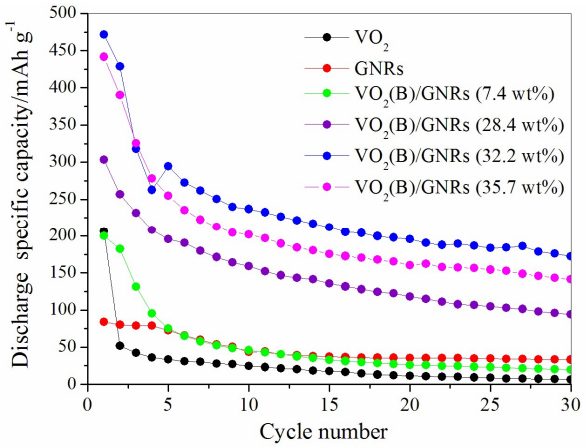

Fig. 7 Discharge specific capacity and cycling performance of VO_2(B)/GNRs composite with the different weight percentages of GNRs.

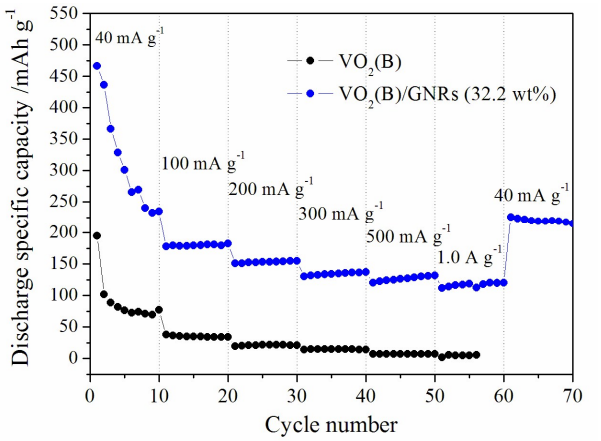

Fig. 8 Rate capabilities of VO_2(B) and VO_2(B)/GNRs (32.2%) composite.

For practical applications, the rate performance is anther critical factor in developing high power lithium ion batteries. The cycling responses of VO_2(B) and VO_2(B)/GNRs (32.2 wt%) composite at different current rates were evaluated and the results are shown in Fig. 8. For VO_2(B), the cycling response became invalid and failed to continue the measure. The discharge specific capacity of VO_2(B)/GNRs (32.2 wt%) composite at 10th cycle with the current rate of 40 mA g^{-1} is 234.5 mAh g^{-1}, and subsequently the average discharge capacity decreases to 179.8, 153.0, 134.2, and 126.4 mAh g^{-1} when the current rate increases to 100, 200, 300 and 500 mA g^{-1}, respectively. Even at a higher current rate of 1.0 A g^{-1}, the reversible capacity of composite still remains 116.9 mAh g^{-1}. Remarkably, a specific capacity of 225.6 mAh g^{-1} is still possible when the current rate is finally returned to 40 mA g^{-1} again, which also suggests the remarkable reversibility of VO_2(B)/GNRs composite material.

Conclusions

Monoclinic VO_2(B) nanoflower and VO_2(B)/GNRs composite were prepared by hydrothermal method at 180 °C for 24 h by using the moderate $H_2C_2O_4$ reductant to reduce V_2O_5. Compared to VO_2(B), the discharge specific capacities and the cycling stabilities can be improved by graphene support, especially VO_2(B)/GNRs. The weight percentage of GNRs affects on the discharge specific capacity and the capacity retention rate of composite. Therein, VO_2(B)/GNRs (32.2 wt%) exhibits the excellent electrochemical performance with the high first discharge specific capacity of 471.5 mAh g^{-1} and the good rate performance. GNRs with a excellent electrical property effectively enhance the electrochemical performance of VO_2(B) cathode material for lithium-ion batteries.

Acknowledgements

This work was supported by National Natural Science Foundation of China (No. 51272044, 61008040, J1103303), Natural Science Foundation of Fujian Province (No. 2013J01180), and Development Foundation of Science and Technology of Fuzhou University (No. 2014-XQ-9).

References

1 S. Megahed and B. Scrosati, *J. Power Sources*, 1994, 51, 79.
2 H. Li, Z. X. Wang, L. Q. Chen and X. J. Huang, *Adv. Mater.*, 2009, 21, 4593.
3 A. Kannan and A. Manthiram, *Solid State Ionics*, 2003, 159, 265.
4 J. X. Li, Y. Zhao, N. Wang, Y. H. Ding and L. H. Guan, *J. Mater. Chem. A*, 2012, 22, 13002.
5 J. S. Sakamoto and B. Dunn, *J. Electrochem. Soc.*, 2002, 149, A26.
6 Y. X Tang, X. H. Rui, Y. Y. Zhang, T. M. Lim, Z. L. Dong, H. H. Hng, X. D. Chen, Q. Y. Yan and Z. Chen, *J. Mater. Chem. A*, 2013, 1, 82.
7 Y. F. Zhang, A, Q, Pan, S. Q. Liang, T. Chen, Y. Tang and X. P. Tan, *Mater. Lett.*, 2014, 137, 174.
8 D. L. Chao, C. G. Zhu, X. H. Xia, J. L. Liu, X. Zhang, J. Wang, P. Liang, J. Y. Lin, H. Zhang, Z. X. Shen and H. J. Fan, *Nano Lett.*, 2015, 15, 565.
9 N. A. Chernova, M. Roppolo, A. C. Dillon and M. S. Whittingham, *J. Mater. Chem.*, 2009, 19, 2526.
10 W. Tang, L. L. Liu, Y. S. Zhu, H. Sun, Y. P. Wu and K. Zhu, *Energy Environ. Sci.*, 2012, 5, 6909.
11 S. Y. Zeng, K. B. Tang, T. W. Li, Z. H. Liang, D. Wang, Y. K. Wang, Y. X. Qi and W. W. Zhou, *J. Mater. Chem. C,* 2008, 112, 4836.
12 N. Ding, X. Y. Feng, S. H. Liu, J. Xu, X. Fang, I. Lieberwirth and C. H. Chen, *Electrochem. Commun.* 2009, 11, 538.
13 X. H. Rui, J. X. Zhu, W. L. Liu, H. T. Tan, D. H. Sim, C. Xu, H. Zhang, J. Ma, H. H. Hng, T. M. Lim and Q. Y. Yan, *RSC Adv.* 2011, 1, 117.
14 H. Q. Li, P. He, Y. G. Wang, E. Hosono and H. S. Zhou, *J. Mater. Chem.*, 2011, 21, 10999.

15 C. Z. Wu, J. Dai, X. D. Zhang, J. L. Yang, F. Qi, C. Gao and Y. Xie, *Angew. Chem. Int. Ed.*, 2010, 49, 134.
16 I. Mjejri, N. Etteyeb and F. Sediri, *Mater. Res. Bull.*, 2014, 60, 97
17 H. B. Zhao, L. Y. Pan, S. Y. Xing, J. Luo and J. Q. Xu, *Journal of Power Sources*, 2013, 222, 21.
18 Y. Sun, S. B. Yang, L. P. Lv, I. Lieberwirth, L. C. Zhang, C. X. Ding and C. H. Chen, *Journal of Power Sources*, 2013, 241, 186.
19 C. Nethravathi, B. Viswanath, J. Michael and M. Rajamath, *Carbon*, 2012, 50, 4839.
20 I. Mjejri, N. Etteyeb and F. Sediri, *Ceram. Int.*, 2014, 40, 1387.
21 S. D. Zhang, Y. M. Li, C. Z. Wu, F. Zheng and Y. Xie, *J. Phys. Chem. C*, 2009,113, 15058.
22 C. V. S. Reddy, E. H. Walker, S. A. W. Sr., Q. L. Williams and R. R. Kalluru, *Curr. Appl. Phys.*, 2009, 9, 1195.
23 W. T. Jiang, J. Ni, K. Yu and Z. Q. Zhu, *Appl. Surf. Sci.*, 2011, 257, 3253.
24 J. J. Huang, X. F. Wang, J. F. Liu, X. M. Sun, L. Wang and X. M. He, *Int. J. Electrochem. Sci.*, 2011, 6, 1709.
25 G. Armstrong, J. Canales, A. R. Armstrong and P. G. Bruce, *J. Power Sources*, 2008, 178, 723.
26 H. M. Liu, Y. G. Wang, K. X. Wang, E. J. Hosono and H. S. Zhou, *J. Mater. Chem.*, 2009, 19, 2835.
27 X. M. Yang, Z. P. Liu, X. D. Li, Z. M. Zhang, L. X. Ji and J. G. Deng, *J. Inorg. Mater.*, 2015, 30, 443.
28 G. Nagaraju and S. Ashoka, *Mater. Charact.*, 2012, 68, 58.
29 C. J. Niu, J. S. Meng, C. H. Han, K. N. Zhao, M. Y. Yan and L. Q. Mai, *Nano Lett.*, 2014, 14, 2873.
30 M. M. Rahmana, J. Z. Wang, N. H. Idris, Z. X. Chen and H. K. Liu, *Electrochim. Acta*, 2010, 56, 693.
31 Y. Liu, B. H. Zhang, Y. Q. Yang, Z. Chang, Z. B. Wen and Y. P. Wu, *J. Mater. Chem. A*, 2013, 1, 13582.
32 T. Qian, N. Xu, J. Q. Zhou, T. Z. Yang, X. J. Liu, X. W. Shen, J. Q. Liang and C. L. Yan, *J. Mater. Chem. A*, 2015, 3, 488.
33 A. L. M. Reddy, M. M. Shaijumon, S. R. Gowda and P. M. Ajayan, *Nano Lett.,* 2009, 9, 1002.
34 H. Zhang, G. P. Cao, Z. Y. Wang, Y. S. Yang, Z. J. Shi and Z. N. Gu, *Nano Lett.,* 2008, 8, 2664.
35 L. B. Hu, W. Chen, X. Xie, N. A. Liu, Y. Yang, H. Wu, Y. Yao, M. Pasta, H. N. Alshareef and Y. Cui, *ACS Nano*, 2011, 5, 8904.
36 H. Jiang, C. Z. Li, T. Sun and J. Ma, *Nanoscale*, 2012, 4, 807.
37 C. Z. Yan, Z. Chen, Y. T. Peng, L. Guo and Y. F. Lu, *Nanotechnology*, 2012, 23, 475701.
38 Y. Shi, S. L. Chou, J. Z. Wang, H. J. Li, H. K. Liu and Y. P. Wu, *J. Power Sources*, 2013, 244, 684.
39 S. B. Yang, Y. J. Gong, Z. Liu, L. Zhan, D. P. Hashim, L. L. Ma, R. Vajtai and P. M. Ajayan, *Nano Lett.*, 2013, 13, 1596.
40 S. Dutta and S. K. Pati, *J. Mater. Chem.*, 2010, 20, 8207.
41 M. Sprinkle, M. Ruan, Y. Hu, J. Hankinson, M. Rubio-Roy, B. Zhang, X. Wu, C. Berger, W. A. Heer and W. A. de Heer, *Nature Nanotechnol.*, 2010, 5, 727.
42 N. F. Zhuang, C. C. Liu, L. N. Jia, L. Wei, J. D. Cai, Y. L. Guo, Y. F. Zhang, X. L. Hu, J. Z. Chen, X. D. Chen and Y. X. Tang, *Nanotechnology*, 2013, 24, 325604.
43 X. Y. Huang, Z. H. Fan, C. L. Lin, L. N. Jia, B. W. Lin, J. Q. Wang, X. L. Hu and N. F. Zhuang, *J. Nanopart. Res.*, 2015, 17, 97.